IEEE Access
Multidisciplinary ⋮ Rapid Review ⋮ Open Access Journal

Received 10 February 2023, accepted 9 March 2023, date of publication 16 March 2023, date of current version 22 March 2023.

Digital Object Identifier 10.1109/ACCESS.2023.3258220

RESEARCH ARTICLE

Wideband Polarization Independent Resonant Cavity Antenna for 6G Applications

MEHRAB RAMZAN AND PADMANAVA SEN, (Senior Member, IEEE)
Barkhausen Institut, 01187 Dresden, Germany

Corresponding author: Mehrab Ramzan (mehrab.ramzan@barkhauseninstitut.org)

This work is financed on the basis of the budget passed by the Saxon State Parliament.

ABSTRACT In this paper, a planar polarization independent resonant cavity antenna (RCA) is proposed to achieve higher gain with a single patch connection instead of using antenna arrays with additional feeding losses. The planar metasurface is based on sub-wavelength complementary circular metallic patches, which provide the same magnitude and phase response for both TE and TM polarized waves. In order to excite the metasurface, an aperture coupled antenna with a circular patch is used to make its integration easier with the metasurface. The proposed antenna design works from 8.97 GHz to 13.1 GHz with a measured 3dB gain bandwidth of 24.2% and it is used to increase the antenna's gain from 8 dBi up to 14.67 dBi. The RCA achieves the measured bandwidths (input matching <-10 dB) above 4 GHz or 37.4%, among the highest reported in the literature with 2 layers.

INDEX TERMS High gain, partial reflecting surface, resonant cavity antenna, wideband.

I. INTRODUCTION

Joint communication and sensing (JC&S) is the central platform for connecting and coordinating billion of devices in the future 6G wireless communication systems [1]. The antenna is the core constituent in the RF front end of these integrated systems and it is accountable for transmitting and receiving electromagnetic waves. The conventional techniques of making an array of an antenna in order to increase the antenna's gain suffer from the substrate and complex feeding network losses [2], [3]. Therefore, there is a growing need to explore alternative and novel approaches to enhance the antenna's gain by minimizing the losses and feeding complexities, especially at the millimeter wave frequencies in order to decrease the path loss and maximize the link margin. For this work, X-band, which can be the future enabler frequency band of 6G applications, is used as the potential frequency band to validate the design.

Metamaterials composed of sub-wavelength resonating unit cell structures with unique properties cover a wide variety of different applications such as high gain resonant cavity antennas (RCA) [2], increasing isolation with electromagnetic bandgaps (EBG) [4], high impedance surfaces (HIS) [5], and miniaturized antennas [6]. However, metamaterials suffer from narrowband properties and these properties are polarization dependent [2]. In this paper, we have proposed a wideband polarization independent planar complementary metasurface based on complementary sub-wavelength circular metallic structures showing a constant phase response over a bandwidth of more than 3.7 GHz. The designed metasurface is utilized to enhance the realized gain of the aperture coupled antenna from 8 dBi to maximum 14.67 dBi excluding the feeding network challenges. The metasurface and aperture coupled antenna are fabricated, and integrated together. Finally, the EM simulations and measured results are compared and a close agreement is found between them.

Section II will describe the design, fabrication and measurement results of the resonant cavity antenna (RCA). Finally, the conclusion of the paper is discussed in section III.

II. ANTENNA AND METASURFACE

This section is divided into three subsections. The first subsection gives a detailed overview of the unit cell simulations and extracted magnitude and phase characteristics of the planar metasurface. In the second subsection, the planar metasurface is integrated with the aperture coupled antenna to

The associate editor coordinating the review of this manuscript and approving it for publication was Shah Nawaz Burokur.

show its focusing characteristics over a wide frequency range. In the third subsection, the simulation and measured results of the RCA are compared.

A. UNIT CELL SIMULATIONS

The initial phase of evaluating the metasurface is carried out using unit cell simulations while defining the master-slave boundary conditions in the HFSS EM environment as shown in Fig. 1. The planar metasurface is composed of two layers of complementary structures consisting of sub-wavelength symmetrical circular patches. It is designed on a single Rogers 4003C substrate with a thickness of 0.813 mm. Fig. 1 shows the unit cell block of the 2D metasurface with the corresponding highlighted master and slave boundary conditions in the HFSS EM design environment. The unit cell dimensions are 8 mm (Uc_x) x 8 mm (Uc_y) with a top circular patch having a radius of 3.45 mm (Uc_{R2}) and the bottom layer consists of an inductive layer made by using circular slots with a radius of 3.15 mm (Uc_{R1}) as shown in Fig. 1 (top and bottom sides of the unit cell). The overall summary of the optimized parameters of the unit cell is given in Table 1.

TABLE 1. RCA optimized dimensions.

Parameters	Antenna (mm)	Metasurface (mm)
L_s	64	64
W_s	64	64
L_p	25	-
W_p	25	-
R_p	5.1	-
L_f	32	-
W_f	1.82	-
L_{stub}	1.2	-
W_{SL}	0.9	-
L_{SL}	5.6	-
h_p	2	-
h	-	16
Uc_x	-	8
Uc_y	-	8
Uc_{R1}	-	3.15
Uc_{R2}	-	3.45
t	0.813	0.813

The circular structure is chosen for the metasurface because of its symmetry. The unit cell is analyzed with respect to different excited modes (TE and TM polarized waves) by using the Floquet ports in the HFSS EM simulation environment as shown in Fig. 2. The reflection and transmission coefficients of the metasurface with respect to TE and TM polarized waves are shown in Fig. 3. The identical results of the reflection and transmission coefficients with respect to TE and TM polarized waves show that the metasurface is polarization independent when it is excited with respect to different polarized waves. Moreover, the reflection coefficient phase of the metasurface with respect to TE and TM waves is shown in Fig. 3 and the -180 degrees phase requires that the metasurface should be placed $\lambda/2$ far away from the H-slot.

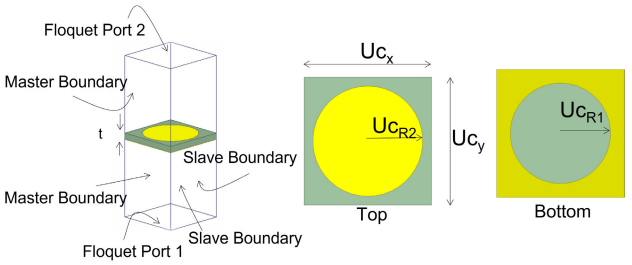

FIGURE 1. Polarization independent wideband metasurface unit cell with highlighted boundary conditions in the EM environment.

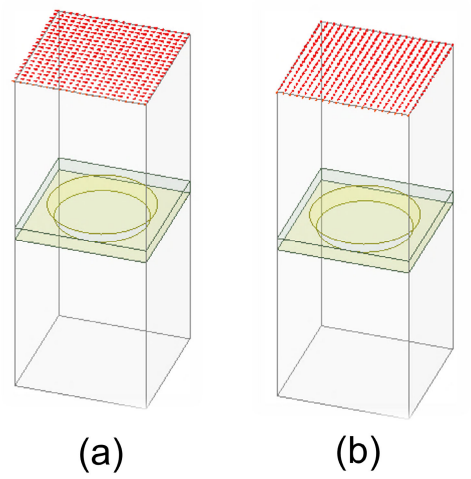

FIGURE 2. Different excited modes using Flouquet ports (a) TE mode (b) TM mode.

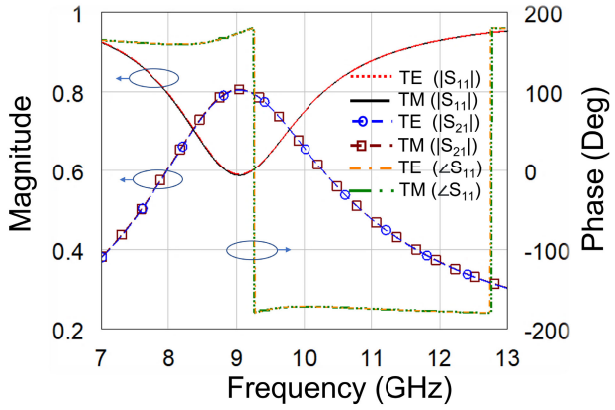

FIGURE 3. Simulation results of the magnitude and phase of the wideband metasurface with respect to TE and TM polarized waves.

B. RCA SIMULATIONS

Fig. 4 shows the overall resonant cavity antenna (RCA) with different layers. A wideband slot antenna with a circular patch is used to excite the planar metasurface. The circular patch is kept at a height of 2 mm above the slot to maximize the bandwidth of the antenna. In order to have broadband characteristics, an H-slot is used in the ground and it is excited

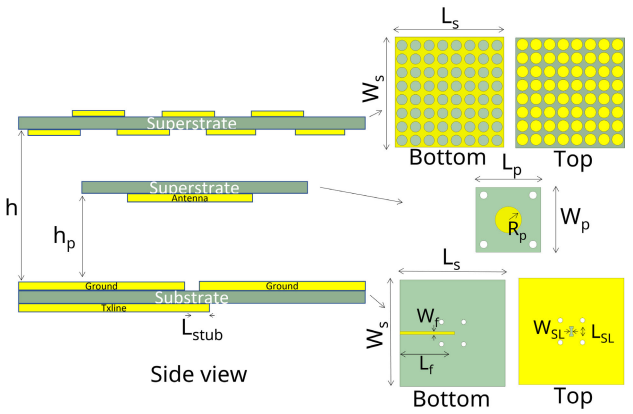

FIGURE 4. Wideband polarization independent resonant cavity antenna (RCA) with different layers.

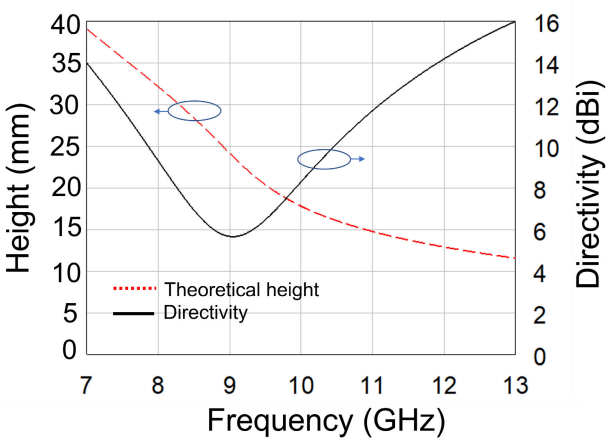

FIGURE 5. Computed height and directivity offered by the metasurface based on the simulated phase and reflection coefficient of unit cell.

with a 50-ohm transmission line at the bottom of the antenna with an additional stub length (L_{stub}) to ensure maximum coupling to the circular patch antenna. The different optimized parameters of the proposed RCA are shown in Table 1. According to equation 1 [2], the metasurface should be placed $\lambda/2$ away from the slot antenna provided that the reflections from the ground are 180 degrees (Φ_g) and the metasurface introduces a -180 degree (Φ_m) phase shift (N considered as 1). The estimated theoretical height of the metasurface with respect to different frequencies is shown in Fig. 5, which implies at the lower frequencies, the variation of the height is higher, and this variation becomes less at the higher frequencies. On the other side, the gain of the antenna is dependent on the magnitude of the reflection coefficient as given in equation 2. The theoretically computed directivity with frequency offered by this metasurface is shown in Fig. 5, which indicates an increasing trend of directivity in the frequency regime between 9 GHz to 13 GHz. The total directivity is composed of a summation of the directivity offered by the slot antenna plus the directivity by the metasurface. Considering these variations and the wideband nature of the RCA, the metasurface is placed at a distance of 16 mm above the slot antenna to have a good impedance matching over a bandwidth of around 3.8 GHz. The realized gain also depends highly on this height (h) separation. Lowering it increases the gain at higher frequencies but at the expense of compromising the impedance matching at lower frequencies.

$$h + t\sqrt{\epsilon_r} = \frac{(\Phi_m + \Phi_g)\lambda}{4\pi} + \frac{N\lambda}{2} \quad N = 0, \pm1, \pm2, .. \quad (1)$$

$$D = 10 \log \frac{1 + |\Gamma|}{1 - |\Gamma|} \quad (2)$$

The different factors controlling the input matching of the resonant cavity antenna are also demonstrated in this paper. During these simulations, all the other parameters are set to optimized values, and the influence of the corresponding dimension is recorded on the input reflection of the resonant cavity antenna. The input reflection coefficient response of the resonant cavity antenna (RCA) at different integration levels is shown in Fig. 6. The input reflection coefficient shows two possible resonances without the integration of the patch and the metasurface. As the patch antenna is placed 2 mm above the H-slot, the antenna offers better matching and one extra resonance. Finally, the integration of the top metasurface creates two additional resonances and brings the input reflection below −10 dB covering a frequency bandwidth of 3.8 GHz, as illustrated in Fig. 6.

The influence of the additional stub (with length L_{stub}) used near the H-slot on the input reflection coefficient of the RCA is shown in Fig. 7. This stub facilitates matching the antenna and its length is chosen large enough, around 1.2 mm to match the integrated antenna over a wide frequency range, especially at the lower frequency band. An investigation was carried out on the H-slot length (L_{SL}) by varying it from 3.6 mm to 4 mm and its influence was observed on the reflection coefficient of the RCA as shown in Fig. 8. The H-slot length variation has only an impact on the resonance frequency at a lower frequency and the optimized value for this slot length is observed to be 3.8 mm which gives good matching and maximum coverage over the wide frequency range.

Moreover, the influence of the circular patch radius (R_p) is also recorded on the input reflection coefficient of the RCA as depicted in Fig. 9. It can be clearly seen that the circular patch mainly influences the third and last resonance of the RCA. Therefore, its value is chosen to be 5.1 mm to keep the reflection coefficient below −10 dB over a wide frequency range. The height of the metasurface plays a crucial role in deciding its gain in correspondence to good matching. The influence of the metasurface height (h) on the input reflection coefficient of the RCA is demonstrated in Fig. 10. In order to have wideband matching, h is chosen to be 16 mm. Although lower values of h can increase the gain performance of the RCA at higher frequencies, as shown in Fig. 11. However, the matching starts getting worse on the other side.

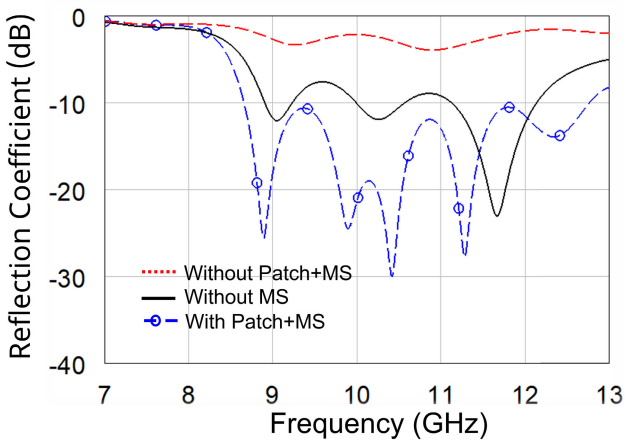

FIGURE 6. Input reflection coefficient of the RCA with respect to different integration layers (with and without circular patch and metasurface (MS)).

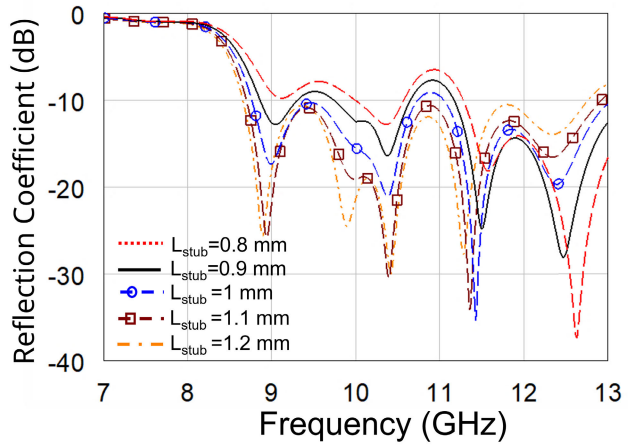

FIGURE 7. The effect of the additional stub length (L_{stub}) on the input reflection coefficient of the RCA.

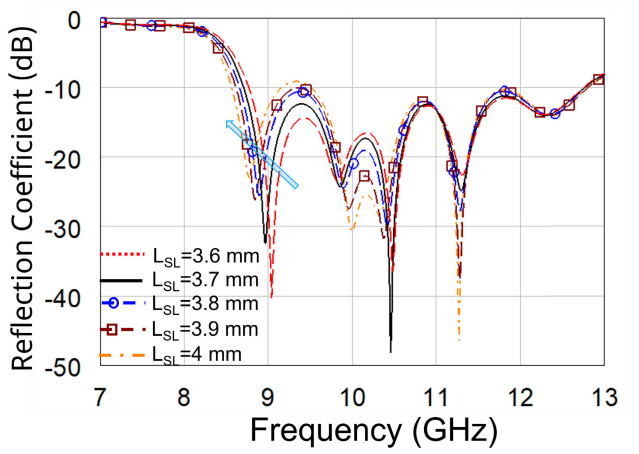

FIGURE 8. Input reflection coefficient of the RCA with respect to different length (L_{SL}) variations of the H-slot.

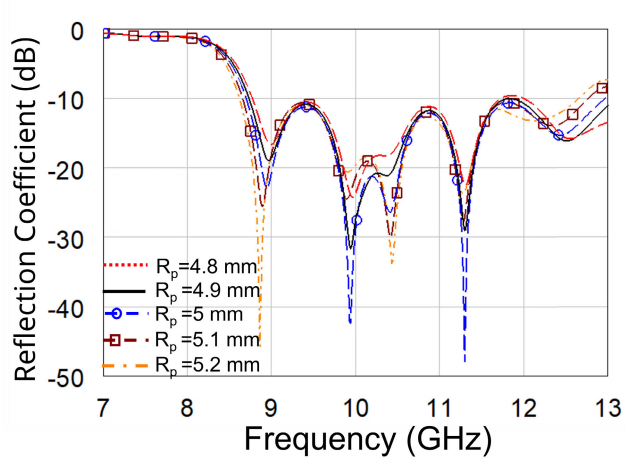

FIGURE 9. Input reflection coefficient of the RCA with respect to different radius (R_P) of the circular patch.

The metasurface is also analyzed with respect to different polarizations by aligning the slot in horizontal and vertical directions, as shown in Fig. 12. The results are illustrated in Fig. 13, which shows both polarizations have exactly the same behavior on the input reflection coefficient of the antenna. Furthermore, the gain values over the frequency also show that the metasurface increases the gain of the antenna identically, as shown in Fig. 13. Moreover, the polarization independent behavior of the RCA can be realized by rotating the metasurface unit cells with respect to the feeding antenna. Fig. 14 shows the rotation of the circular unit cells has a negligible effect on the reflection coefficient of the antenna. On the other side, the maximum realized gain of the antenna also remains constant considering these unit cells' rotations as shown in Fig. 15.

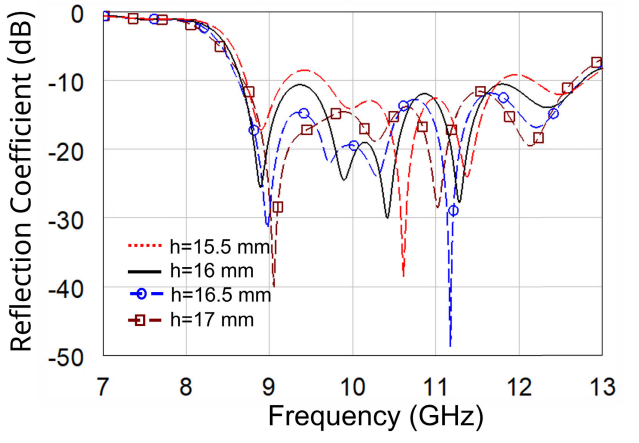

FIGURE 10. Different cases of the input reflection coefficient of the RCA with respect to the metasurface height variations.

C. FABRICATION AND MEASUREMENTS

Fig. 16 shows the top and bottom view of the fabricated wide-band RCA. The different layers were integrated and aligned using plastic spacers at the corner of the boards. Fig. 17 shows the simulated and measured reflection coefficient of

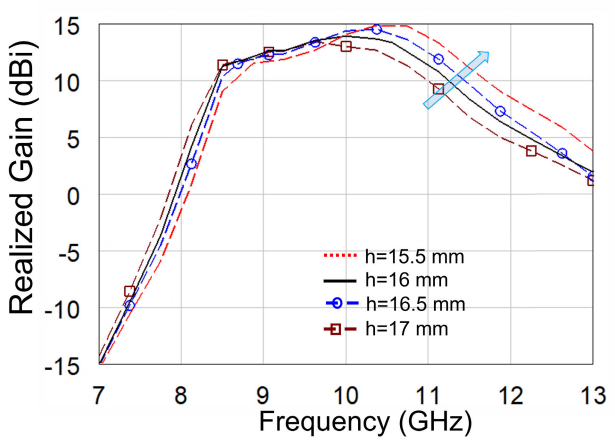

FIGURE 11. Different cases of the realized gain with respect to different metasurface height variations.

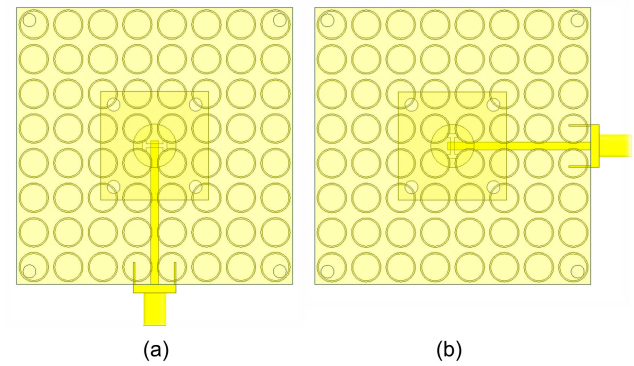

FIGURE 12. The metasurface excited with two different polarizations (a) Horizontal slot (b) Vertical slot.

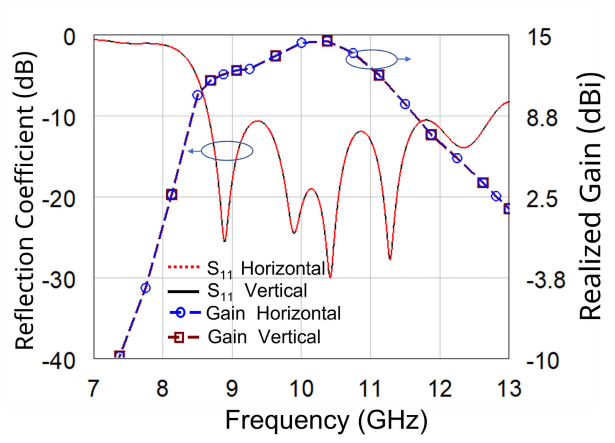

FIGURE 13. Reflection coefficient and realized gain of the RCA with respect to (a) Horizontal slot (b) Vertical slot.

the antenna. The antenna shows a measured impedance bandwidth of 4.13 GHz (37.4%) from 8.97 GHz to 13.1 GHz. There are a few discrepancies and frequency shifts in the measured results compared to the simulation results, primarily

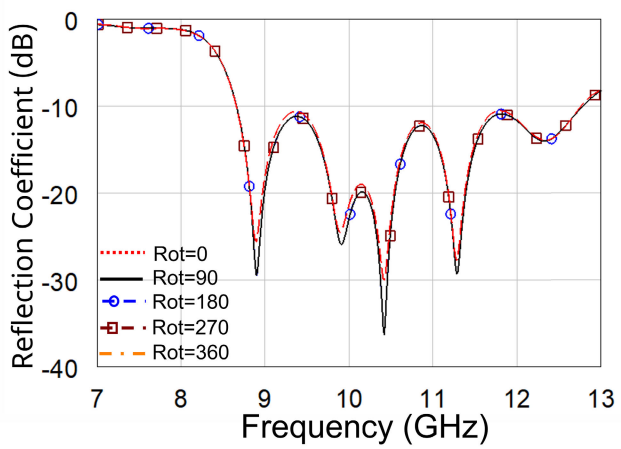

FIGURE 14. Reflection coefficient of the RCA with different rotation of the unit cells with respect to the feeding antenna.

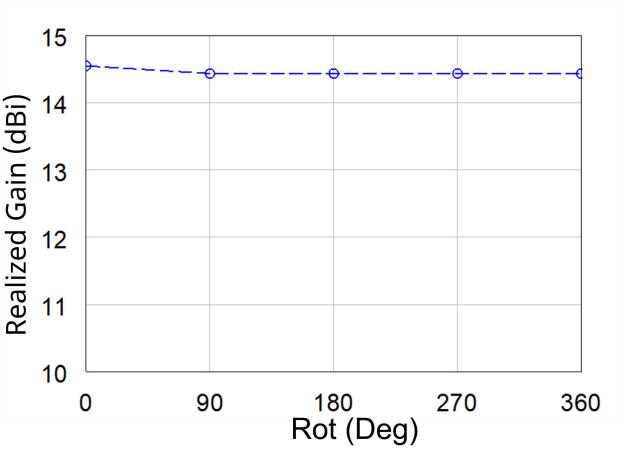

FIGURE 15. Maximum realized gain of the RCA with respect to different rotation of the unit cells with respect to the feeding antenna.

due to the fabrication tolerance. However, the measured input matching results (S_{11}) are below -10 dB and have a close agreement with the simulation results in the operating frequency range. The measured realized gain of the antenna over frequency is also shown in Fig. 18. This confirms that the metasurface can increase the gain of the antenna up to 14.67 dBi in the regime of 10.56 GHz. The measured gain results (max gain 14.7 dBi) also show the same pattern except for the slight shift in the results owing to the shift in the measured reflection coefficient. The surface current distribution on the top and bottom surfaces of the metasurface is shown in Fig. 19. It shows maximum magnitude at the center and decaying behavior at the edges which comply with the broadside radiation phenomenon.

The radiation pattern of the RCA in the E-plane and H-plane is also measured at different frequencies to show its directive behavior. Fig. 20, Fig. 21, and Fig. 22 show the comparison of the RCA's measured and simulated radiation pattern at 9 GHz, 10 GHz and 11 GHz, respectively. There

TABLE 2. Comparison of the proposed RCA with the other published articles.

Ref.	Feed	Size (λ_0)	BW (%)	M.Gain (dBi)	SLL (dB)	HPBW	R. Ef.	A Ef.	3dB BW (%)	P.I	L
[2]	Probe	2.83 x 2.83 x 0.5	0.55+0.78	16	<-13	18°	91.38	39.5	-	No	1
[7]	1 Patch	4.43 x 4.43 x 0.062	3.15	15.8	NA	30°	NA	15.4	-	No	2
[8]	WG slot	1.9 x 1.9 x 0.5	21.5	16.1	NA	NA	-	78.6	21.5	No	2
[9]	WG slot	2.4 x 2.4 x 0.66	-	14	-18	>30°	NA	34.6	32.3	-	4
[10]	2x2 Array	1.55 x 1.55 x 0.11	24.3	12.5	-20	NA	-	53.7	-	-	2
[11]	2x2 Array	2.8 x 2.8 x 0.5	26.9	15.7	<-10	25°	86.8	37.7	-	-	2
[12]	Cavity Slot	2.98 x 2.65	12	18.4	-	-	95	68	-	No	-
[13]	Ms Slot	2.2 x 2.2 x 0.54	25	13.92	-	-	-	40.5	-	-	2
[14]	Ms Slot	2.76 x 2.76 x 0.5	15.5	13.78	-	-	-	25	18.7	-	2
T.W	Ms H-slot	2.25 x 2.25 x 0.55	36.2	14.67	<-14.24	28°	94	46	24.8	Yes	2
T.W1	Ms H-slot	2.25 x 2.25 x 0.55	25	16.53	<-14.24	26°	97	70.7	13.5	Yes	2
T.W2	Ms H-slot	2.25 x 2.25 x 0.55	37.4	14.7	<-14.24	28°	94	46.4	24.2	Yes	2

$^{\lambda_0}$ Center frequency wavelength, $^{T.W}$ This work (Simulated without shield), $^{T.W1}$ This work (Simulated with shield), $^{T.W2}$ This work (Measured without shield), ^{WG} Waveguide, ^{Ms} Microstrip, ^{BW} -10 dB Impedance bandwidth, ^{SLL} Side lobe level, ^{HPBW} Half power beam width, $^{R.Ef.}$ Radiation Efficiency (%), $^{A.Ef.}$ Aperture Efficiency (%), $^{P.I}$ Polarization independent, ^{3dBBW} 3dB Gain bandwidth (S_{11}<-10 dB), ^{L} No. of layers

FIGURE 16. Fabricated Wideband polarization independent RCA (a) Top view (b) Bottom view.

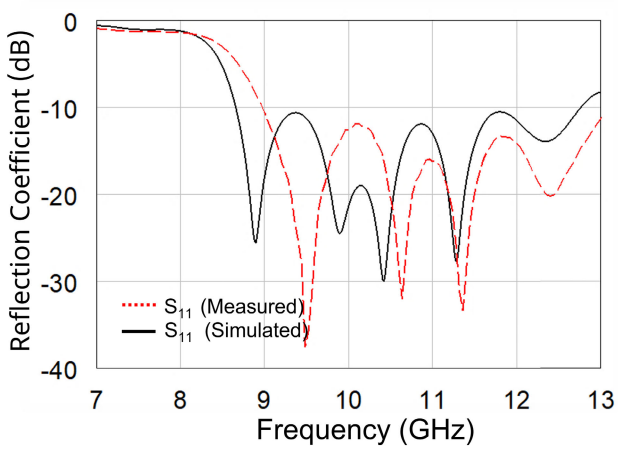

FIGURE 17. Measured and simulated reflection coefficient results of the wideband RCA.

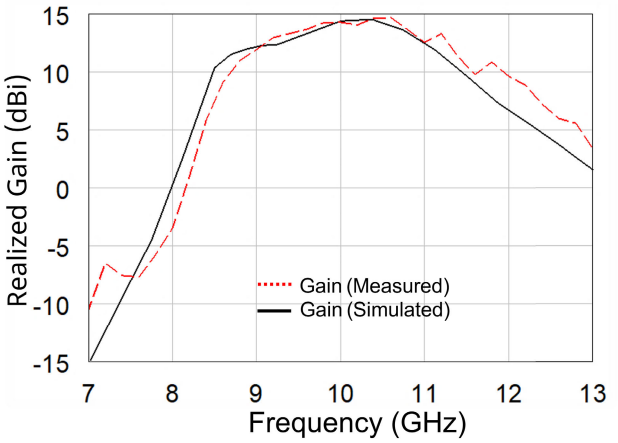

FIGURE 18. Measured and simulated realized gain of the wideband RCA with respect to frequency.

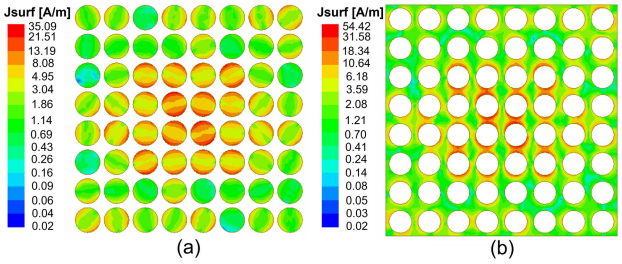

FIGURE 19. Surface current distribution on the (a) top and (b) bottom surface of the metasurface at 10 GHz.

is a close agreement between the results except for some discrepancies in the E-plane owing to the non-ideal environment and reflections from the positioner and its limited angular resolution in the elevation plane.

Table 2 shows a detailed comparison of the proposed work with other recently published research work in terms of different antenna parameters. While comparing with [9], it was found that its 3dB gain bandwidth is a bit higher than our design, but the metasurface presented consists of 4 layers and it is fed with a waveguide-fed slot which makes it bulky and difficult to integrate for future portable 6G applications. Moreover, its aperture efficiency is less than 35%. Compared with the other two layer designs, it is evident that the metasurface is polarization independent with a 3dB wideband gain and impedance bandwidth characteristics. In addition to that, the maximum radiation efficiency of the antenna is higher than 92% as compared to other reported designs. The

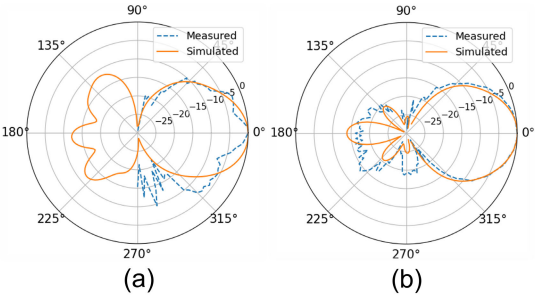

FIGURE 20. Comparison of the 2D radiation pattern of the RCA (measured and simulated) in the (a) E-Plane (b) H-Plane at 9 GHz.

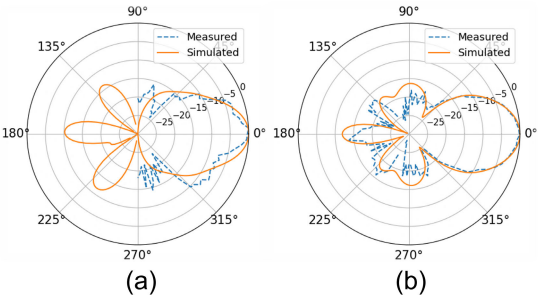

FIGURE 21. Comparison of the 2D radiation pattern of the RCA (measured and simulated) in the (a) E-Plane (b) H-Plane at 10 GHz.

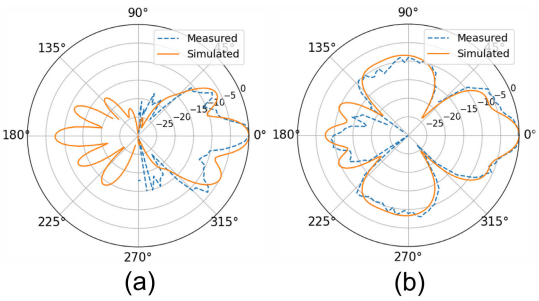

FIGURE 22. Comparison of the 2D radiation pattern of the RCA (measured and simulated) in the (a) E-Plane (b) H-Plane at 11 GHz.

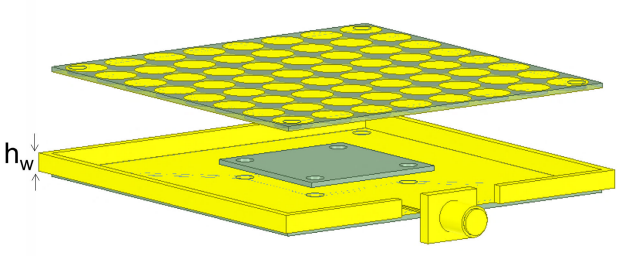

FIGURE 23. Resonant cavity antenna with a vertical conducting wall connected to the ground plane.

maximum aperture efficiency of the antenna can be further increased by lowering the height of the metasurface but at the expense of decreasing the impedance bandwidth and 3dB

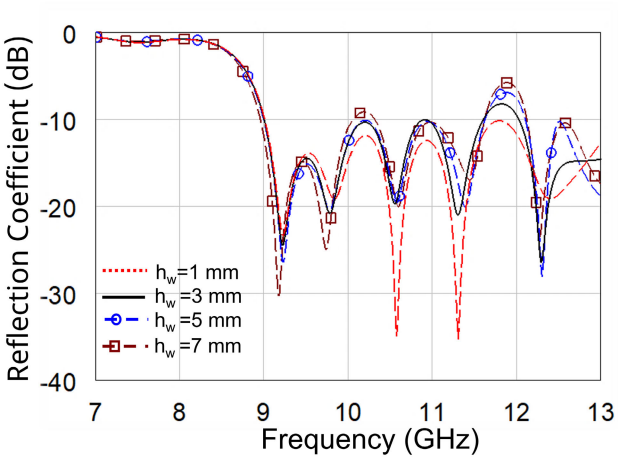

FIGURE 24. Input reflection coefficient of the resonant cavity antenna (RCA) with respect to the height of the surrounding vertical ground wall.

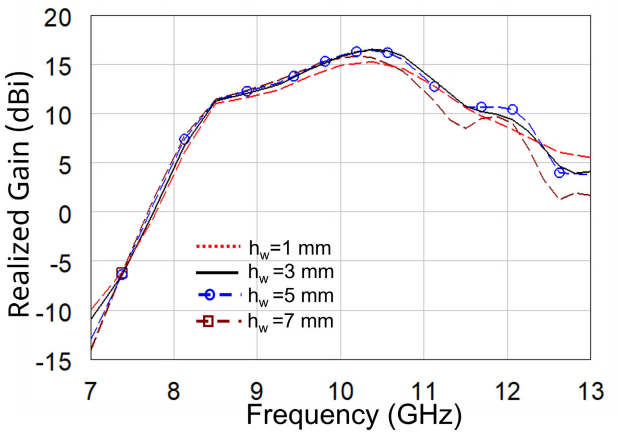

FIGURE 25. Realized gain of the resonant cavity antenna (RCA) with respect to the height of the surrounding vertical ground wall.

gain bandwidth of the antenna. The maximum aperture efficiency of the resonant cavity antenna can also be increased to 70.7% as given in Table 2 by enclosing it with a 3 mm high vertical metallic shielded wall connected to the ground plane as shown in Fig 23. However, in that case, the 3dB gain bandwidth of the antenna will be decreased, as depicted in Fig. 24 and Fig. 25, respectively.

III. CONCLUSION

This work presents a wideband and high gain resonant cavity antenna that can experimentally work in the frequency range of 8.97 GHz to 13.1 GHz with the fractional impedance bandwidth and 3dB gain bandwidth of 37.4% and 24.2%, respectively. Moreover, given the symmetrical nature of the metasurface, it is shown that the antenna shows identical results if the polarization of the H-slot is changed from horizontal to vertical. As a future work, the tapered version of the metasurface will be analyzed to decrease the sidelobe level

further. A special investigation will be done with the tapered surface to keep the gain constant over the 4 GHz frequency bandwidth.

ACKNOWLEDGMENT

The authors would like to acknowledge the contribution of Tim Hentschel and Gerhard Fettweis to this work.

REFERENCES

[1] C. D. Lima, "Convergent communication, sensing and localization in 6G systems: An overview of technologies, opportunities and challenges," *IEEE Access*, vol. 9, pp. 26902–26925, 2021.
[2] M. Ramzan and P. Sen, "Dual-band gain-boosted planar lens antenna using a single layer metasurface for 6G applications," in *Proc. Joint Eur. Conf. Netw. Commun. 6G Summit (EuCNC/6G Summit)*, Jun. 2022, pp. 446–450.
[3] A. Hassanien, W. Swelam, and M. H. A. El Azeem, "16×8 wideband microstrip planar array antenna for E-band millimeter-wave 5G high speed WLAN and broadband internet applications," in *Proc. IEEE Int. Symp. Antennas Propag. USNC/URSI Nat. Radio Sci. Meeting*, Jul. 2017, pp. 2613–2614.
[4] M. Ramzan, A. N. Barreto, and P. Sen, "Meta-surface boosted antenna to achieve higher than 50 dB TRX isolation at 26 GHz for joint communication and radar sensing (JC&S)," in *Proc. 16th Eur. Conf. Antennas Propag. (EuCAP)*, Mar. 2022, pp. 1–5.
[5] F. Costa, S. Genovesi, and A. Monorchio, "On the bandwidth of high-impedance frequency selective surfaces," *IEEE Antennas Wireless Propag. Lett.*, vol. 8, pp. 1341–1344, 2009.
[6] S. A. Rezaeieh, M. A. Antoniades, and A. M. Abbosh, "Miniaturization of planar Yagi antennas using Mu-negative metamaterial-loaded reflector," *IEEE Trans. Antennas Propag.*, vol. 65, no. 12, pp. 6827–6837, Dec. 2017.
[7] A. Ghasemi, S. N. Burokur, A. Dhouibi, and A. de Lustrac, "High beam steering in Fabry–Pérot leaky-wave antennas," *IEEE Antennas Wireless Propag. Lett.*, vol. 12, pp. 261–264, 2013.
[8] A. Lalbakhsh, M. U. Afzal, K. P. Esselle, S. L. Smith, and B. A. Zeb, "Single-dielectric wideband partially reflecting surface with variable reflection components for realization of a compact high-gain resonant cavity antenna," *IEEE Trans. Antennas Propag.*, vol. 67, no. 3, pp. 1916–1921, Mar. 2019.
[9] M. W. Niaz, Y. Yin, R. A. Bhatti, Y.-M. Cai, and J. Chen, "Wideband Fabry–Pérot resonator antenna employing multilayer partially reflective surface," *IEEE Trans. Antennas Propag.*, vol. 69, no. 4, pp. 2404–2409, 2021.
[10] S. Jagtap, A. Chaudhari, N. Chaskar, S. Kharche, and R. K. Gupta, "A wideband microstrip array design using RIS and PRS layers," *IEEE Antennas Wireless Propag. Lett.*, vol. 17, no. 3, pp. 509–512, Mar. 2018.
[11] C. Yang, X. Zhu, and P. Liu, "A circularly polarized Fabry–Pérot resonant cavity antenna using frequency selective surface-based partial reflecting surface," *Int. J. RF Microw. Comput.-Aided Eng.*, vol. 31, no. 8, Aug. 2021, Art. no. e22735.
[12] R.-S. Chen, "High-efficiency and wideband dual-resonance full-metal cavity-backed slot antenna array," *IEEE Antennas Wireless Propag. Lett.*, vol. 19, no. 8, pp. 1360–1364, Aug. 2020.
[13] F. Meng and S. K. Sharma, "A wideband resonant cavity antenna with compact partially reflective surface," *IEEE Trans. Antennas Propag.*, vol. 68, no. 2, pp. 1155–1160, Feb. 2020.
[14] M. A. Meriche, H. Attia, A. Messai, S. S. I. Mitu, and T. A. Denidni, "Directive wideband cavity antenna with single-layer meta-superstrate," *IEEE Antennas Wireless Propag. Lett.*, vol. 18, no. 9, pp. 1771–1774, Sep. 2019.

MEHRAB RAMZAN received the B.S. degree in telecommunication engineering from the FAST National University of Computer and Emerging Sciences, Pakistan, in 2011, and the M.S. degree in electrical and electronics engineering from Bilkent University, Ankara, Turkey, in 2015. From November 2016 to March 2020, he was a Research Associate with the Chair of RF and Photonics Engineering, TU Dresden, Germany. Since April 2020, he has been a Research Associate with Barkhausen Institut, Dresden, Germany. He has authored or coauthored over 16 journals and conference papers. His research interests include the development of resonant cavity antennas, metasurfaces, metamaterials, frequency-selective surfaces, implanted antennas, miniaturized antennas, and matching networks.

PADMANAVA SEN (Senior Member, IEEE) received the B.Tech. degree in electronics and electrical communication engineering from the Indian Institute of Technology Kharagpur, India, in 2003, and the M.S. and Ph.D. degrees from Georgia Institute of Technology, Atlanta, GA, USA, in 2005 and 2007, respectively. In 2010, he joined Broadcom Corporation, Irvine, CA, USA, where he worked for six years toward the development of phased array systems at 60-GHz frequency bands (802.11ad). Apart from Broadcom Corporation (Irvine, USA, and Bengaluru, India), he was with a 60-GHz startup Sayana Wireless, Atlanta, for three years, and with IBM Corporation, VT, USA, for one year. In 2018, he has joined Barkhausen Institut, Dresden, Germany, where he is currently leading the RF Design Enablement Group, with focus on joint communications and sensing. He has authored or coauthored over 50 IEEE journals and conference papers. He holds three issued U.S. patents.